Conductivity reconstruction algorithms and numerical simulations for magneto–acousto–electrical tomography with piston transducer in scan mode*

Guo Liang(郭 亮)[a)b)c)†], Liu Guo-Qiang(刘国强)[a)‡], Xia Hui(夏 慧)[a)], Liu Yu(刘 宇)[a)], and Lu Min-Hua(陆敏华)[d)]

[a)] *Institution of Electrical Engineering, Chinese Academy of Sciences, Beijing* 100190, *China*
[b)] *University of Chinese Academy of Sciences, Beijing* 100190, *China*
[c)] *College of Control Theory and Engineering, China University of Petroleum, Qingdao* 266580, *China*
[d)] *Guangdong Key Laboratory for Biomedical Measurements and Ultrasound Imaging, Shenzhen* 518060, *China*

(Received 4 March 2014; revised manuscript received 2 April 2014; published online 10 August 2014)

Conductivities tomography with the interactions of magnetic field, electrical field, and ultrasound field is presented in this paper. We utilize a beam of ultrasound in scanning mode instead of the traditional ultrasound field generated by point source. Many formulae for the reconstruction of conductivities are derived from the voltage signals detected by two electrodes arranged somewhere on tissue's surface. In a forward problem, the numerical solutions of ultrasound fields generated by the piston transducer are calculated using the angular spectrum method and its Green's function is designed approximately in far fields. In an inverse problems, the magneto–acousto–electrical voltage signals are proved to satisfy the wave equations if the voltage signals are extended to the whole region from the boundary locations of transducers. Thus the time-reversal method is applied to reconstructing the curl of the reciprocal current density. In addition, a least square iteration method of recovering conductivities from reciprocal current densities is discussed.

Keywords: magneto–acousto–electrical tomography, Green's function, conductivity reconstructing, scan mode

PACS: 43.35.Rw, 43.40.At, 43.20.Bi **DOI:** 10.1088/1674-1056/23/10/104303

1. Introduction

Magneto–acousto–electric tomography (MAET), as a conductivity imaging method, has received much attention from many researchers and is expected to have a clinical usage. In order to obtain the conductivities of tissues, the electrical impedance tomography (EIT)[1,2] and magnetic induction tomography (MIT)[3] could be used, though the resolutions of EIT and MIT are much lower than that of the ultrasonograph. On the other hand, only when the density of tissues is changed to a certain extent, will the ultrasonic methods be effective. MAET combines the advantages of electrical methods in acquiring conductivities and the strong point of ultrasound in high spatial resolution. It could help doctors to recognize the tiny abnormal conductivity value as an indication of tumour.

Ultrasound waves which are applied to tissues could generate vibrations of ions. When the moving ions are under the action of homogeneous magnetic field, they can experience a Lorenz force and form the source currents dispersed in the area.

The voltage signals generated by the source currents can be detected by two electrodes arbitrarily arranged in the area.[4] On the other hand, if the two electrodes and magnetic fields are kept unchanged, and the ultrasound field as input and voltage signal as output are exchanged, the same tasks can be performed. That is to say, if the currents are injected into the medium by two electrodes, the Lorentz forces caused by the currents in the magnetic field would create mechanical vibrations. Thus, the ultrasound pressure signals can be detected around the area. Reconstruction can also be achieved by the ultrasound pressure signals, which is called magneto–acoustic tomography (MAT).[5–7]

The forward and inverse problems of MAET are well studied substantially by Elena *et al.*,[8] Leonid,[9] and Jensen and Svendsen.[5] Furthermore, the different frequencies of ultrasound are used by Haider *et al.*[10] in DF-MAET for solving the problems of weak signals in the area of homogeneous conductivities. Leonid[9] has reconstructed the conductivities by curls of the reciprocal current densities. This is done by the hypothesis that the ultrasound waves are similar to the δ function and satisfy reciprocity theorem. Generally speaking, in order to reconstruct the conductivities, the reconstruction of the curls of reciprocal current densities is necessary. Most

*Project supported by the National Natural Science Foundation of China (Grant Nos. 51137004, 51277169, and 61271424).
†E-mail: guoliang@upc.edu.cn
‡Corresponding author. E-mail: gqliu@mail.iee.ac.cn
© 2014 Chinese Physical Society and IOP Publishing Ltd

of the above methods are based on the Green's function of point source in infinite area and impulse function along time axis. As the ultrasound waves originating from a point source propagate in all directions, the electrodes will experience the ultrasound waves and cause unexpectedly large MAE signals. If we apply piston transducers or focused transducers in scan mode, the ultrasound waves can be well controlled in certain directions. However, the tomography for plane ultrasound in MAET is seldom reported. In this paper, we first derive the expressions of ultrasound field generated by piston transducers, and give a kind of Green's function approximately in the far field. Next, we show that the MAE voltage signals satisfy the wave equations like ultrasound pressures.

Therefore, the time reversal algorithm with the Green's function mentioned above could be used for fast reconstructions. In the latter case, we introduce the algorithm of recovering current densities from curls of current densities by Helmholtz theorem. After that, an iterative least square method is formulated to reconstruct conductivities from current densities. The results of numerical simulations in two dimensions show the effectiveness and higher resolutions of the series algorithms.

2. Ultrasonic transducer analysis

Unfocused transducers in medical ultrasound imaging are mostly piston transducers, which can be equivalent to the plane ultrasound sources. The piston transducers are also the basic units for generating ultrasound of B mode. If the vibration velocity distribution on the surface of the plane is known with certain angular frequency ω, the angular spectrum of the source can be represented as follows:

$$S(\omega,k_x,k_y) = (1/2\pi)\iint w(\omega,x',y') \times \exp(-\mathrm{i}k_x x' - \mathrm{i}k_y y')\,\mathrm{d}x'\,\mathrm{d}y'. \quad (1)$$

Here $w(\omega,x',y')$ is the vibration velocity function of point (x',y') on the surface of the plane source with $z=0$. The k_x and k_y are the numbers of waves along x and y axes. It is obvious that the angular spectrum is the Fourier transform of the velocity fields in two dimensions.

Therefore the ultrasound pressure field can be represented by following the research result given by Lin *et al.*[12] as follows:

$$P(\omega,x,y,z) = (\omega\rho/2\pi)\iint S(\omega,k_x,k_y) \exp(\mathrm{i}k_x x + \mathrm{i}k_y y + \mathrm{i}k_z z)/k_z\,\mathrm{d}k_x\,\mathrm{d}k_y. \quad (2)$$

Here ρ is the mass density of the medium. By apodization technology, the vibration of piezoelectric crystal with Gaussian distribution can be easily generated. The vibration velocity function on source plane could be expressed as follows:

$$w(r) = w(x',y') = A\exp\{-[(x'-x_0)/x_r]^2 - [(y'-y_0)/y_r]^2\}, \quad (3)$$

where (x',y') represents the point on source plane and A represents the amplitude of vibration velocity. By substituting Eq. (3) into Eqs. (2) and (1), we obtain the distributions of ultrasound pressures along x and y axes with different values of propagating distance z.

For simplicity, considering the x–o–z plane with $y=0$ in two dimensions, figure 1 shows the ultrasound pressures with the results calculated by Eqs. (1)–(3). We obtain the similar results to those given by Jensen.[5] According to the features of the ultrasound pressures, we demonstrate a kind of Green's function of velocity potential generated by plane source for a certain angular frequency ω as follows:

$$g(r,t|r_0,0) = \exp\{-[(x'-x_0)/x_r]^2 - [(y'-y_0)/y_r]^2\}\cdot\delta(t-|z-z_0|/c). \quad (4)$$

Here r_0 represents the location of the center point on source plane with coordinate (x_0,y_0,z_0); x_r and y_r are variances of the Gaussian distribution along each axis; c is the ultrasound propagating velocity. It is worth noticing that the Green's function only satisfies the specific angular frequency ω approximately in the far field. This is because the ultrasound pressures have the features mentioned above only for single frequency ω. It can be considered to be approximately suitable for piezoelectric crystal with narrow frequency band.

Equation (4) satisfies the following equation with boundary condition:

$$\begin{cases} g_{tt} = c^2\nabla_n^2 g, & r\in\Omega, \\ g_t|_{t=0} = c^2 w(r)\delta(r-r_\Sigma), & r\in\Omega, \\ g = 0, & r\in\partial\Omega. \end{cases} \quad (5)$$

Here, Ω is the region with the boundary $\partial\Omega$, and is the area that we are to reconstruct; r_Σ represents the sources plane Σ; ∇_n^2 is the Laplace operator along normal direction of source plane.

The Green's function $g(r,t)$ represents the plane wave propagating along the n direction, perpendicular to the source plane, and is stimulated by Dirac function in a time domain.

If the plane wave travels along the axis z, ∇_n^2 would equal $\partial^2/\partial^2 z$. Thus equation (5) describes a plane wave generated by piston transducer travelling along the z direction, which has the distribution like $w(x,y)$ along the x and y axes.

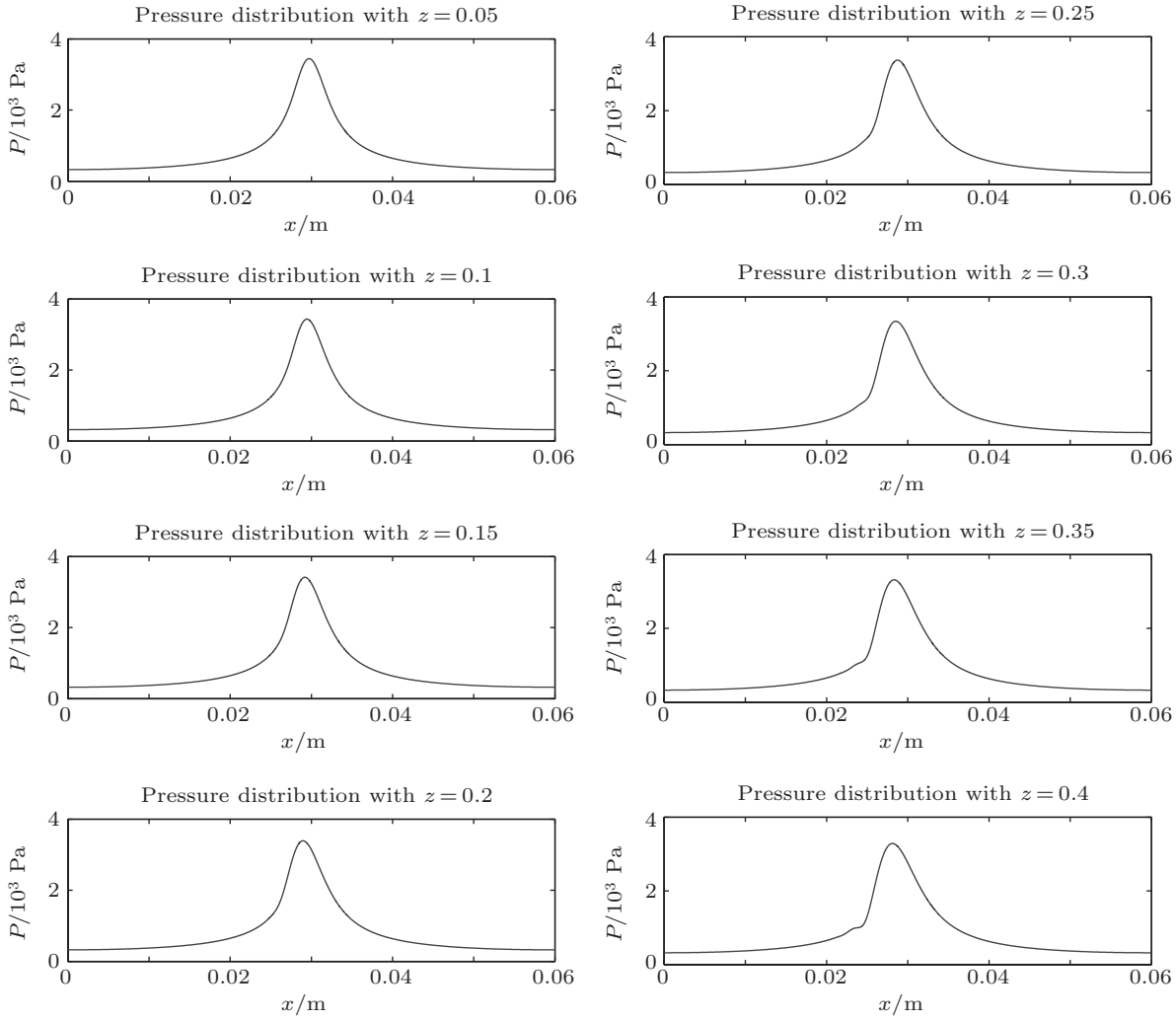


Fig. 1. Ultrasound pressure distributions versus x for different values of propagating distance z when y equals 0. The parameters x_r and y_r both equal 1 mm, x_0 and y_0 both equal 30 mm. The coefficient A in Eq. (3) equals one at a frequency of 1 MHz. The scope of ultrasound changes little and the amplitude of pressure is nearly constant with propagating direction z.

3. Ultrasonic and electromagnetic coupling fields

3.1. Reciprocal theorem and reciprocal current density

When a beam of ultrasound is propagating in a conductive area under the homogenous magnetic field, the vibration of ions $V(r,t)$ would generate the source current

$$\boldsymbol{J}_{\mathrm{e}} = \sigma \boldsymbol{V}(r,t) \times \boldsymbol{B}. \tag{6}$$

Therefore, the electric potential field can be represented by the following formula:

$$\nabla \cdot (\sigma \nabla u - \boldsymbol{J}_{\mathrm{e}}) = 0. \tag{7}$$

The field variable u between two specific points can be measured at two locations of the electrodes. Alternatively, if one ampere of current is injected through the two electrodes, the reciprocal potential field u' can be determined by the following equation:

$$\begin{cases} \nabla \cdot \sigma \nabla u' = \delta(r - r_A)\delta(r - r_B), & r \in \Omega, \\ \partial u'/\partial n = 0, & r \in \partial\Omega, \end{cases} \tag{8}$$

where r_A and r_B are the location of the two electrodes and δ represents the Dirac function of point source. According to reciprocal theorem, the MAE signals can be represented by the following spatial integral as mentioned in Leonoid's paper:[9]

$$u_A^{r_d}(t) - u_B^{r_d}(t) = u_{AB}^{r_d}(t) = \int_{\Omega} \boldsymbol{B} \cdot \boldsymbol{J}'(r) \times \boldsymbol{V}(r,t)\, \mathrm{d}r. \tag{9}$$

Here, $\boldsymbol{J}'(r) = -\sigma \nabla u'$ is the reciprocal current density caused by injecting 1 A of current from r_A and r_B, $V(r,t)$ is the vibration velocity caused by the ultrasound, B is the static magnetic field, ρ is the mass density of medium, and $u_{AB}^{r_d}(t)$represents the MAE voltage signal that is caused by the ultrasound transducer located at r_d and detected by the electrodes at r_A and r_B.

Introduce the velocity potential function $\phi(r,t)$ satisfying:

$$\boldsymbol{V}(r,t) = \nabla \phi(r,t)/\rho, \tag{10}$$

and substituting Eq. (10) into Eq. (9), the resulting equation can be rewritten as[9]

$$u_{AB}^{r_d}(t) = \int_{\Omega} \boldsymbol{B} \cdot \nabla \times J'(r) \phi\,(r,t)\,\mathrm{d}r/\rho. \tag{11}$$

It is easy to prove that the velocity potential function satisfies the same wave equation as ultrasound pressure function. Thus, the $\phi(r,t)$ can be represented by the convolution of Green's function and source functions

$$\phi\,(r,t) = g\,(r,t|r_d,0) * f(t), \tag{12}$$

where r_d represents the location of ultrasound transducer, symbol $*$ refers to the convolution of time, and $f(t)$ is the source function with independent time variable t. Substituting Eq. (12) into Eq. (11), we obtain[14–16]

$$u_{AB}^{r_d}(t) = f\,(t) * \left[\boldsymbol{B} \cdot \int_{\Omega} \nabla \times \boldsymbol{J}'(r) \mathrm{g}\,(r,t|r_d,0)\,\mathrm{d}r/\rho\right]. \tag{13}$$

It is common that the source function $f(t)$ is known for specific ultrasound transducer.

Thus the inner part of the brackets in Eq. (13) can be represented by the de-convolution of $u_{AB}^{r_d}(t)$ and $f(t)$.

3.2. Time-reversal method of reconstructing the curl of reciprocal current density

Now we focus on Eq. (13). If we extend the variable r_d to the whole region Ω and rewrite variable r_d as r', the spatial integral $[\int_{\Omega} \boldsymbol{B} \cdot \nabla \times \boldsymbol{J}'(r) \mathrm{g}\,(r,t|r_d,0)\,\mathrm{d}r]/\rho$ is the integral solutions of the following problem according to Leonid[9]

$$\begin{cases} u\,(r',t)_{tt} = c^2 \nabla_n^2 u(r',t), & r' \in \Omega, \\ u\,(r',t)_t|_{t=0^+} = [c^2 B \cdot \nabla \times J'(r')]/\rho, & r' \in \Omega, \\ u(r',0) = 0, & r' \in \partial\Omega. \end{cases} \tag{14}$$

If $u\,(r',0)_t$ can be reconstructed, $\nabla \times J'(r)$ will be recovered to be pointwise. Thus, the problem of reconstructing $\nabla \times J'(r)$ from the MAE signal is equivalent to the problem of reconstructing the initial value $u\,(r',0)_t$ from Eq. (14). We do this by the boundary values $u_{AB}^{r_d}(t)$, which represent the field variables $u\,(r',t)$ detected at the location r_d imaginarily. Whereas, in fact, $u_{AB}^{r_d}(t)$ is the voltage signals detected by the electrodes located at r_A and r_B. If all r_d values are located at the boundary $\partial\Omega$, encircling the entire region Ω, there are many methods that can reconstruct $u\,(r',0)_t$ from Eq. (14). Equation (14) is the so-called initial value problem (IVP). The time-reversal algorithm is one of the popular methods based on the following statements.

According to the Helmholtz–Kirchhoff integral equation, the time-reversal equation can be represented by Yuan *et al.*[17] as

$$u(r',t) = -2 \int_{T_0}^{t^+} \mathrm{d}t_0 \int [u^{r_d}(t_0) \partial g(r',t|r_d,t_0)/\partial n_n]\,\mathrm{d}s_d. \tag{15}$$

Substituting Eq. (4) into Eq. (15) and taking the derivative of the terms on both sides of the resulting equation at $t = 0$ s, we can obtain the following equation for time-reversal reconstructing:

$$\frac{\partial u(r',0)}{\partial t} = -(2/c) \int \exp\{-[(x'-x_0)/x_r]^2 - [(y'-y_0)/y_r]^2\} u_{AB}^{r_d\,\prime\prime}(|z-z_d|/c)\,\mathrm{d}s_d. \tag{16}$$

Here, $u''^{r_d}_{AB}(t)$ is the second derivative with respect to time t. The second derivatives of all MAE signals are necessary for reconstructing field variable's first derivatives $u\,(r',0)_t$, which are determined by $u(r',0)_t = c^2 \boldsymbol{B} \cdot \nabla \times \boldsymbol{J}'(r)/\rho$ in Eq. (14). By each scan, the contributions of the $u''^{r_d}_{AB}(t)$ to $u\,(r',0)_t$ in Eq. (16) are influenced by the factor

$$\exp\{-[(x'-x_0)/x_r]^2 - [(y'-y_0)/y_r]^2\},$$

which is an exponential function of the distance between the center line of the scanning area and the field point.

3.3. Reconstruction of reciprocal current density

Generally speaking, the reciprocal current density has no divergence. If the curls of current density and the boundary conditions are known, the current density can be reconstructed at each point. Supposing that the curl of current density is reconstructed as $\boldsymbol{K}(r) = \nabla \times \boldsymbol{J}'(r)$ by the method mentioned above, $\boldsymbol{J}'(r)$ is well determined by the following formula according to Hemholz theorem:

$$\begin{cases} \nabla \times \boldsymbol{J}'(r) = K(r), & r \in \Omega, \\ \nabla \cdot \boldsymbol{J}'(r) = 0, & r \in \Omega, \\ \boldsymbol{J}'\,(r) \cdot n = 0, & r \in \partial\Omega/(r_A \text{ and } r_B), \\ \boldsymbol{J}'\,(r_A) \cdot \boldsymbol{n} = \delta\,(r - r_A), & \\ \boldsymbol{J}'\,(r_B) \cdot \boldsymbol{n} = -\delta\,(r - r_B). & \end{cases} \tag{17}$$

For simplicity, the following discussion is mainly about two-dimensional (2D) rectangular region. Thus $J'(r)$ has the x component and the z component, and $\nabla \times J'(r)$ is along the y axis. Therefore, the detailed expressions of Eq. (17) are given as follows:

$$\begin{cases} \partial^2 J'_x/\partial x^2 + \partial^2 J'_x/\partial z^2 = -\partial K/\partial z, & (x,z) \in \Omega, \\ \partial^2 J'_z/\partial x^2 + \partial^2 J'_z/\partial z^2 = \partial K/\partial x, & (x,z) \in \Omega, \\ J'_x = 0, & (x,z) \in \partial\Omega_{\mathrm{LR}}\ /(A \text{ and } B), \\ \partial J'_x/\partial z = -K, & (x,z) \in \partial\Omega_{\mathrm{UD}}\ /(A \text{ and } B), \\ J'_z = 0, & (x,z) \in \partial\Omega_{\mathrm{UD}}\ /(A \text{ and } B), \\ \partial J'_z/\partial x = K, & (x,z) \in \partial\Omega_{\mathrm{LR}}\ /(A \text{ and } B), \\ J'_x(x_A,z_A) = \delta(x - x_A, z - z_A), & \text{if } (x_A,z_A) \in \partial\Omega_{\mathrm{LR}}, \\ J'_x(x_B,z_B) = -\delta(x - x_B, z - z_B), & \text{if } (x_B,z_B) \in \partial\Omega_{\mathrm{LR}}, \\ J'_z(x_A,z_A) = \delta(x - x_A, z - z_A), & \text{if } (x_A,z_A) \in \partial\Omega_{\mathrm{UD}}, \\ J'_z(x_B,z_B) = -\delta(x - x_B, z - z_B), & \text{if } (x_B,z_B) \in \partial\Omega_{\mathrm{UD}}. \end{cases} \tag{18}$$

Here, (x_A,z_A) and (x_B,z_B) represent the locations of the two electrodes respectively; $\partial\Omega_{\mathrm{LR}}$ represents the left and right

boundary along the x axis; and $\partial\Omega_{\mathrm{UD}}$ represents the upper and lower boundary along the z axis; δ is Dirac function in two dimensions. Therefore, J_x' and J_z' can be well recovered by solving Eq. (17).

3.4. Reconstruction of conductivities

Reconstructing σ from $\boldsymbol{J}'(r)$ is a work of iteration by least square method. If the area is divided into n small square regions and the conductivity σ is constant in each small region, the objective functional can be established as follows:

$$Q(\sigma) = \sum_{i=1}^{n} \int_{\Omega} \left| \boldsymbol{J}^M(r) - \boldsymbol{J}'(r) \right|^2 \mathrm{d}r, \tag{19}$$

where $\boldsymbol{J}'(r)$ is the numerical result of the forward process of calculating Eq. (8) and $\boldsymbol{J}^M(r)$ is the reciprocal current density reconstructed by Eq. (17). In order to minimize the objective functional, σ_i can be obtained by the following equation in each square region Ω_i:[18]

$$\sigma_i = -\int_{\Omega_i} \boldsymbol{J}^M(r) \cdot \nabla u' \,\mathrm{d}\Omega \Big/ \int_{\Omega_i} \nabla u' \cdot \nabla u' \,\mathrm{d}\Omega$$
$$i = 1, 2, 3, \ldots, n. \tag{20}$$

Therefore, the steps of iterations should be taken as follows.

Step 1 Solve the boundary value problem Eq. (8) with any given distribution of conductivity σ_i by FD or FE method, and then work out the result of Eq. (19). If the result of Eq. (19) is less than predefined errors, the iterations should stop, otherwise go to Step 2.

Step 2 Substitute ∇u into Eq. (20) and refresh σ_i in each small region. Go back to Eq. (8) with new σ_i for refreshing ∇u and $\boldsymbol{J}'(r)$.

Step 3 Calculate Eq. (19) and compare the obtained result with predefined errors. If $Q(\sigma) <$ error, iteration should be terminated, otherwise go to Step 2.

4. Methods and numerical experiments

The numerical experiments are performed in the 0.03 m $\times$ 0.06 m rectangular model of xoz plane. The ultrasonic velocity potential function has the form of the first derivative of Gaussian function with a frequency of 1 MHz and the spatial resolution along the propagation direction is about 1.5 mm, which is as short as the wave length. The distribution of velocity on source plane follows Eq. (3), where x_r equals 0.005 m, x_0 equals $k\Delta x$ and y equals y_0. For each scan of time k, the center point of source plane holds the same coordinate y_0, moves along the x axis in length steps of $\Delta x = 1$ mm and keep a 5-mm distance from the surface of the target area. In practice, because the diameter of source plane is about 5 mm, much larger than the step length along the x axis, the values of σ_i in a certain small region i of many adjacent scans can all make contributions to MAE signal. We assume that the experimental area is filled with homogenous ultrasonic medium with mass density 1000 kg/m^3 and sound velocity 1500 m/s, which is similar to human tissue-like water. The static homogenous magnetic induction intensity $\boldsymbol{B}$ is 0.2-T along the y direction. The sketch map of the experiment is demonstrated as Fig. 2.

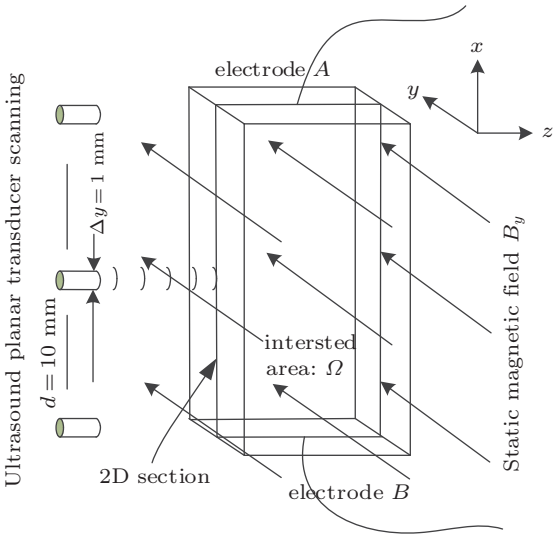


Fig. 2. Sketch map of ultrasound scanning.

The forward process for MAE signals lies in calculating Eqs. (5)–(7), which include the ultrasonic field problem and the electromagnetic fields problem.

Generally speaking, if the forward problem and inverse problem share the same algorithm theoretically, the reconstructing results are hard to be persuasive.

Thus, we choose COMSOL MULTIPHYSCS as the software of finite element method for calculating the MAE signals.

In order to recover the conductivities, the whole area in two dimensions is divided into 30×60 small square regions and each region covers 1 mm^2. The conductivity is considered to be invariable within each of the small square regions.

5. Results

5.1. Smooth conductivity distribution

The curls of current density are reconstructed first by time-reversal method. We focus on the formula: $\nabla \times \boldsymbol{J}'(r) = -\nabla\sigma \times \nabla u'$. The curl of current: $\nabla \times \boldsymbol{J}'(r)$ will be singular if σ is unsmooth. Thus, we choose the smooth conductivities as the target for reconstruction firstly. Even so, the information about $\nabla\sigma$ along the direction of $\nabla u'$ is lost. In order to avoid the loss of $\nabla\sigma$, we should use two pairs of electrodes at different locations to recover the whole information. For simplicity,

despite the absence of specific information along the direction of $\nabla u'$, we can still reconstruct the conductivities only with one pair of electrodes in our simulations.[21]

Figure 3 shows the real values of conductivities, and figure 4 shows the corresponding MAE signals. These signals are stimulated by the ultrasound transducers located at different positions of x from 0 m to 0.06 m. The scanning points are within the same plane of the dashed rectangle in Fig. 2.

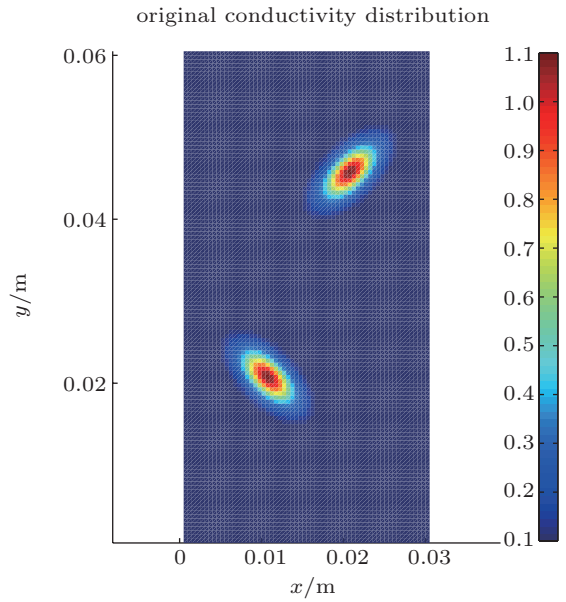


Fig. 3. (color online) Original conductivities from 0.1 S to 1 S with distribution of Eq. (21) in the plane of dashed box in Fig. 2.

The original 2D conductivity distribution function with two abnormal areas of different shapes and positions is described as

$$\begin{aligned}\sigma = {} & 0.1+\exp\{-[(x-x_1)\cos\varphi+(y-y_1)\sin\phi/3]^2/c_1^2 \\ & +[-(x-x_1)\sin\phi+(y-y_1)\cos\varphi/3]^2/c_1^2\} \\ & +\exp\{-[(x-x_2)\cos\varphi+(y-y_2)\sin\phi/3]^2/c_2^2 \\ & +[-(x-x_2)\sin\phi+(y-y_2)\cos\varphi]^2/3/c_2^2\}. \qquad (21)\end{aligned}$$

Each abnormal body follows the Gaussian distribution with variance of $c_1 = c_2 = 0.0009$ m, center points $x_1 = 0.02$ m, $y_1 = 0.045$ m, and $x_2 = 0.01$ m, $y_2 = 0.02$ m respectively. Equation (21) also indicates that the distribution is of coordinate rotation through an angle $\varphi = 45^\circ$ in counterclockwise sense.

The MAE signals in Fig. 4 are detected by plate electrodes placed at the top and bottom surfaces of the model. Here we take into consideration the plate electrodes instead of point electrodes, thereby avoiding the unexpected large signals resulting from the singularity of point source-like Dirac function. It is obvious that the abnormal conductivity regions are consistent with the signal's changes in Fig. 4. At the same time, the signals have some noises with high frequency, which come from the numerical algorithm of FEM.

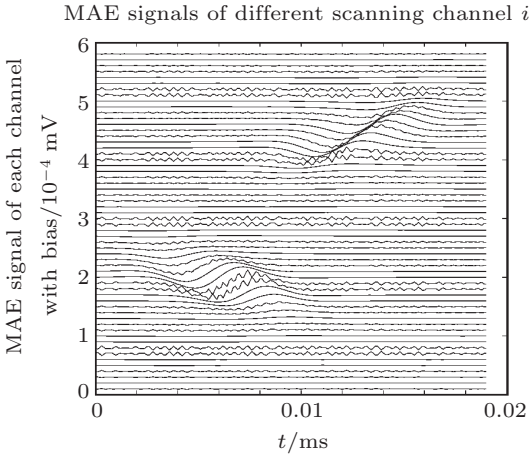


Fig. 4. MAE signals of different scanning channels, detected by plate electrodes. In order to show all the voltages of 58 channels, the signal values of channel i are added by fixing a bias at $10^{-4} \times i$ V.

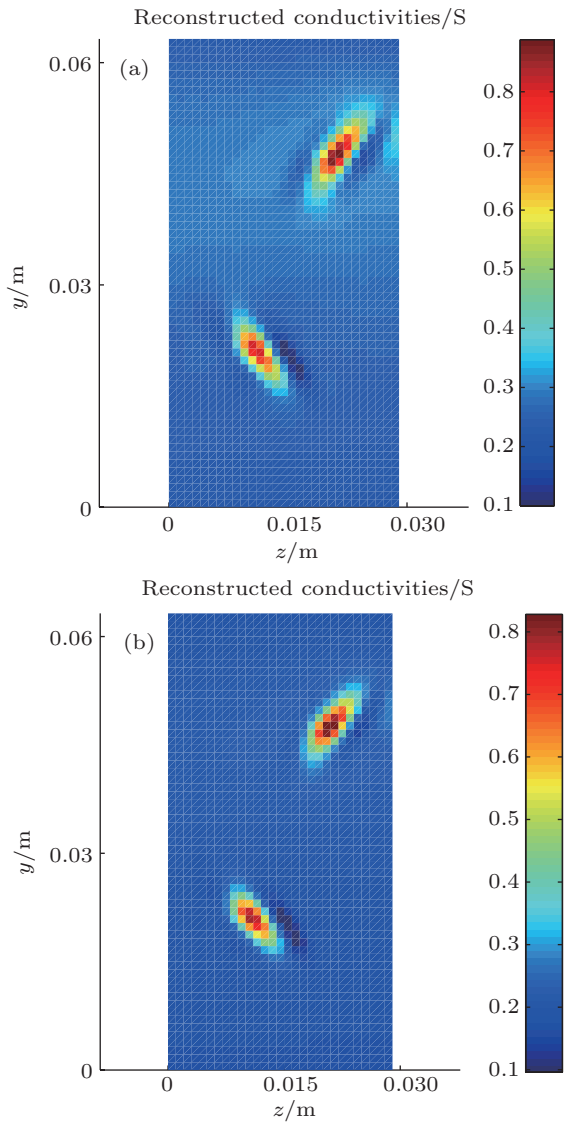


Fig. 5. (color online) Reconstructing results of conductivities, showing the results of 10 (a) and 20 (b) iterations.

We can find in Fig. 5(a) that the abnormal conductivity regions can be clearly displayed and the values of reconstructed conductivities are equal to real values approximately. On the other hand, there are artifacts near the abnormal conductivity areas. With the increase of iteration times, the images quality could be improved and the reconstructed values of conductivities will approach to the real ones.

5.2. Unsmooth conductivities

If the σ is unsmooth, that is, the conductivities in space change more quickly than the wave length of ultrasound, the curls of current will be singular. Thus the absolute values of conductivities are mostly dependent on the scale of mesh grid in inverse problem and cannot be recovered. While in fact, if we project ultrasound waves from the left boundary of the whole regions, the ultrasound vibration directions are all perpendicular to the left and right edges of each small square region. In this case, parts of the edges of different conductivity regions are perpendicular to the directions of the ultrasound vibrations. We will demonstrate the results that the relative distribution of conductivities can also be reconstructed by using our algorithm.

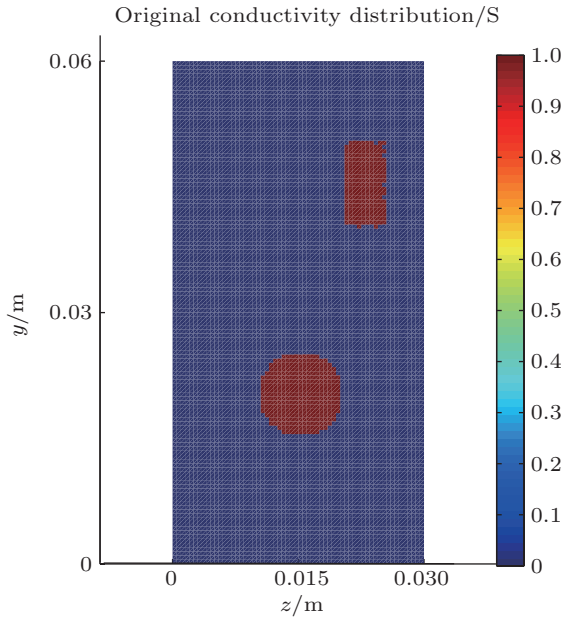


Fig. 6. (color online) Original unsmooth conductivity distribution.

In order to verify the conclusion, we give a real distribution of conductivity as shown in Fig. 6. The reconstructed conductivities are shown in Fig. 7.

Because the absolute values of conductivity cannot be recovered, the normalized conductivities are displayed in Fig. 7. Although the singularity of the curl of current density creates the unexpected large artifacts around the abnormal bodies (especially around the circular abnormal conductivity areas), the abnormal bodies are also easy to distinguish from the background.

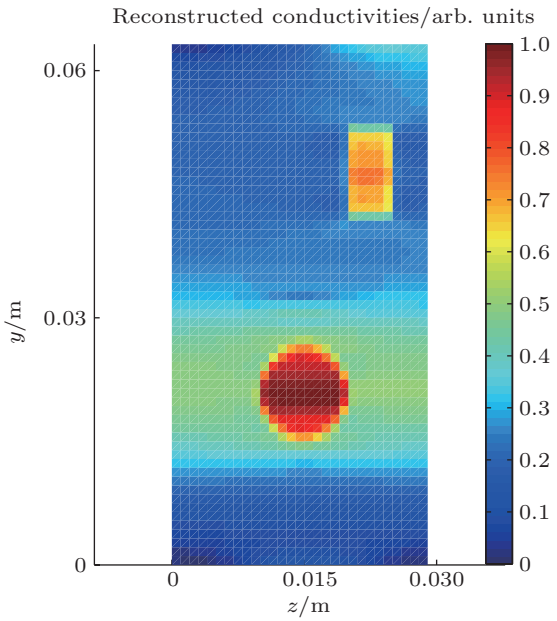


Fig. 7. (color online) Reconstructed conductivities.

6. Conclusions

The MAET is a newly developed method for imaging conductivities, which has both the advantage of high resolution of ultrasound and the advantage of functional tomography of electrical method. In the hypothesis of homogenous ultrasonic medium, the conductivities can be reconstructed by the magneto–acousto–electrical signals of different ultrasonic scannings at different positions around the object or on one side of the object. If the ultrasounds are generated by piston transducers, the specific Green's function is used to calculate the ultrasound fields. Thus the time-reversal method is effective for reconstructing the curl of reciprocal current density. The next work is to reconstruct the conductivities from the curl of current pointwise by using the method derived from Helmholtz theorem and least square iteration.

In order to generate a plane wave, the diameter of piston transducer is much larger than both the wave length of ultrasound and the step length of each scan. Thus the adjacent scans share many same points along x axis, and will result in inaccuracy of the conductivity images. By using the Green's function with Gauss distribution along the direction perpendicular to the vibration, the interference between adjacent scans can be reduced to some extent. Further study should be carried out for inhomogeneous ultrasonic medium using different Green's functions.

References

[1] Paulson K, Lionheart W and Pidcock M 1993 *IEEE Trans. Med. Imag.* **12** 681

[2] Metheral P, Barber D C, Smallwood R H and Brown B H 1996 *Nature* **380** 509

[3] Griffiths H 2001 *Meas. Sci. Technol.* **12** 1126

[4] Han W, Shah J and Balaban R S 1998 *IEEE Trans. Med. Imag.* **45** 119

[5] Jensen J A and Svendsen N B 1992 *IEEE Trans. Ultrason. Ferroelectr. Freq. Control* **39** 262

[6] Li X and He B 2010 *IEEE Trans. Med. Imag.* **29** 1759

[7] Xia R, Li X and He B 2010 *IEEE Trans. Biomed. Eng.* **57** 708

[8] Renzhiglova E, Ivantsiv V and Xu Y 2010 *IEEE Trans. Ultrason. Ferroelect. Freq. Control* **57** 2391

[9] Leonid K 2012 *Inverse Problems* **28** 035002

[10] Haider S, Hrbek A and Xu Y 2008 *Physiol. Meas.* **29** 41

[11] Li Y L, Ma Q Y, Zhang D and Xia R M 2008 *Chin. Phys. B* **17** 4302

[12] Lin W J, Wang X M and Zhang H L 2006 *Chin. J. Geophys.* **49** 284

[13] Zeng X P 2011 "Research for Magneto–Acousto–Electrical Tomography" (M.S. dissertation) (Institute of Electrical Engineering, Chinese Academy of Sciences) (in Chinese)

[14] Guo L, Liu G Q, Xia H and Chen J 2013 *Chin. Phys. Lett.* **30** 124303

[15] Zeng X P, Liu G Q, Xia H and Xu X Y 2010 3*rd International Conference on Biomedical Engineering and Informatics,* October 16–18, 2010, Yantai, China, p. 95

[16] Xu M H, Xu Y and Wang L V 2003 *IEEE Trans. Biomed. Eng.* **50** 814

[17] Xu Y and Wang L V 2004 *Phys. Rev. Lett.* **92** 033902

[18] Liu G Q 2006 *Medical Electromagnetic Imaging* (Beijing: Science Press) p. 143

[19] Liu G Q, Huang X and Xia H 2013 *Chin. Sci. Bull.* **58** 3600

[20] Huang X, Liu G Q and Xia H 2013 *Transaction of China Electrotechical Society* **28** 67 (in Chinese)

[21] Leo M, Li X and He B 2011 *IEEE. Trans. Biomed. Eng.* **58** 713